



Stabilizing chiral spin structures via an alternating Dzyaloshinskii-Moriya interactionJuriaan Lucassen ^{1,*}, Mariëlle J. Meijer,¹ Mark C. H. de Jong,¹ Rembert A. Duine,^{1,2} Henk J. M. Swagten,¹ Bert Koopmans,¹ and Reinoud Lavrijsen^{1,†}¹*Department of Applied Physics, Eindhoven University of Technology, P.O. Box 513, 5600 MB Eindhoven, the Netherlands*²*Institute for Theoretical Physics, Utrecht University, Princetonplein 5, 3584 CC Utrecht, the Netherlands* (Received 1 April 2020; revised 9 July 2020; accepted 10 July 2020; published 29 July 2020)

The stabilization of chiral magnetic spin structures in thin films is often attributed to the interfacial Dzyaloshinskii–Moriya interaction (DMI). Very recently, however, it has been reported that the chirality induced by the DMI can be affected by dipolar interactions. These dipolar fields tend to form Néel caps, which entails the formation of a clockwise chirality at the top of the film and a counterclockwise chirality at the bottom. Here we show that engineering an alternating DMI that changes signs across the film thickness, together with the tendency to form Néel caps, leads to an enhanced stability of chiral spin-structures. Micromagnetic simulations for skyrmions demonstrate that this can increase the effective DMI in a prototypical [Pt/Co/Ir] multilayer system by at least 0.6 mJ m^{-2} . These gains are comparable to what has been achieved using additive DMI, but more flexible as we are not limited to a select set of material combinations. We also present experimental results: By measuring equilibrium domain widths, we quantify the effective DMI in [Pt/Co/Ir] multilayer systems typically used for skyrmion stabilization. Upon introducing an alternating DMI, we demonstrate changes in the effective DMI that agree with our simulations. Our results provide a route toward enhancing the stability of chiral spin structures that does not rely on enlarging the chiral interactions.

DOI: [10.1103/PhysRevB.102.014451](https://doi.org/10.1103/PhysRevB.102.014451)**I. INTRODUCTION**

Magnetic skyrmions are whirling chiral spin structures that can be as small as a few nanometers [1–4]. Because of their topological protection, they are extremely stable magnetic quasiparticles that might find their use in many applications such as magnetic racetrack memory [1–6]. Skyrmions are typically stabilized by the Dzyaloshinskii-Moriya interaction (DMI), which originates from a global inversion symmetry breaking in combination with spin-orbit coupling [7,8]. Although skyrmions exist in many systems [2,9–14], there is a great interest in skyrmions stabilized in ultrathin ferromagnets. Their stabilization is achieved through the interfacial DMI from a symmetry-breaking interface between an ultrathin ferromagnet and a heavy metal [15–17]. In these ultrathin systems, the magnetic properties can be tailored for specific applications by varying the magnetic layer thicknesses and interfaces.

Unfortunately, the DMI is often not large enough to stabilize magnetic skyrmions at room temperature. To compensate for this, the magnetic volume is usually increased to enhance the thermal stability and reduce the skyrmion energy [12–14,18]. The concomitant increase of dipolar interactions, however, has been shown both theoretically and experimentally to compete with the DMI, leading to a nonuniform magnetic chirality across the thickness of the layers [19–28]. This is considered detrimental for applications because most

of the functionality relies on the uniform chirality of a skyrmion across the thickness of the multilayer system [29].

On the other hand, despite their negative effect on the magnetic chirality, even without the DMI, dipolar interactions are able to stabilize so-called dipolar skyrmions [30–32]. This occurs through the formation of Néel caps, which is the formation of a clockwise (CW) chirality at the top of the film and a counterclockwise chirality at the bottom. Inspired by this, we suggest here to combine the formation of Néel caps with a layer-dependent alternating DMI to enhance the stability of chiral spin-structures as is shown schematically in Fig. 1(a) for a magnetic domain wall. The dipolar fields introduce Néel caps with a CW Néel wall at the top of the film, and a counterclockwise (CCW) Néel wall at the bottom. For a uniform DMI, this leads to competition with the DMI across half the stack. Therefore, we intentionally reverse the sign of the DMI halfway through the system, such that in both halves of the stack the DMI field points in the same direction as the dipolar fields, which leads to a reduction in both the domain wall and skyrmion energy. In the first part of this paper, we investigate this principle using MuMax³-based micromagnetic simulations [33] and demonstrate that it leads to significant increases in the effective DMI by comparing skyrmion energies for different DMI configurations. Thereafter, we also present experimental results on the effect of modifying the DMI in a multilayer [Pt/Co/Ir] system. Upon changing the DMI configuration, we find almost a factor of 2 increase in the effective DMI after accounting for growth-induced variations in the magnetic parameters through an averaging approach, which we verify with micromagnetic simulations. This proves that Néel caps can be exploited to significantly increase the stability of chiral spin structures and opens a

*j.lucassen@tue.nl

†r.lavrijsen@tue.nl

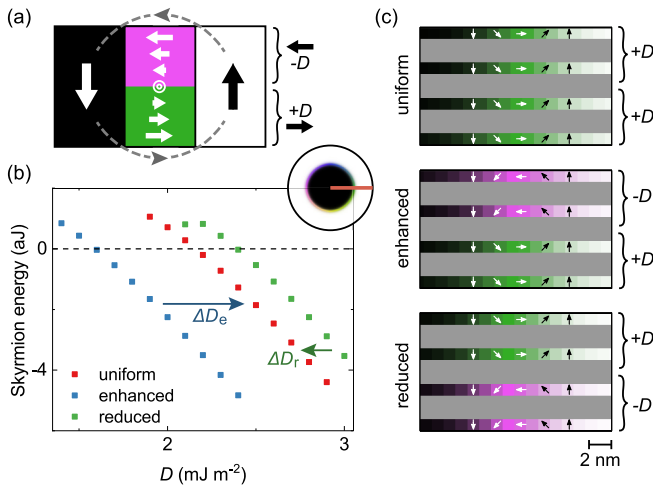


FIG. 1. (a) Schematic overview of the physical interactions exploited to increase the stability of chiral spin structures. The dipolar fields (grey) from the down and up domains (black and white, respectively) create two Néel caps in the domain wall (pink and green). Halfway through the layer, the sign of the DMI D is reversed such that the effective fields of the dipolar interactions are everywhere aligned with the effective field of the DMI (black). The arrows indicate the direction of magnetization and a green (pink) domain wall corresponds to a magnetization pointing to the right (left). (b) Skyrmion energy relative to the uniformly magnetized state as a function of D for the three DMI configurations shown in (c). The arrows indicate the effective DMI gain (ΔD_e) and loss (ΔD_r). The only time a data point is included is when both the uniformly magnetized and skyrmion state are (meta)stable. Inset: Simulation geometry with a skyrmion in a confined dot, where the red horizontal line indicates the profile of a domain wall such as shown in (a) and (c). (c) Stack configurations for the three different DMI configurations with $N = 4$, where we show the resulting cross section of a skyrmion profile using the arrows for $N = 4$ and $D = 2.2$ mJ m⁻². The dark-grey regions correspond to the nonmagnetic layers and the colors are as in (a).

way to tailor them by modifying magnetic interactions on a layer-by-layer basis.

II. MICROMAGNETIC SIMULATIONS

We investigate the behavior of confined magnetic skyrmions in a 256-nm-diameter circular dot [inset Fig. 1(b)] with MuMax³ using [NM(2)/FM(1)] \times N systems, with N repeats of a 1-nm-thick ferromagnetic layer (FM) sandwiched in between 2-nm-thick nonmagnetic (NM) spacer layers. The magnetic parameters used for these calculations correspond to the experimental parameters of the prototypical [Pt/Co/Ir] systems experimentally investigated later in this paper. More details on the simulations can be found in Supplemental Material note I [34]. In Fig. 1(b), the energy of the skyrmion state with respect to the uniformly magnetized state is plotted as a function of the DMI D for three different DMI configurations which are indicated in Fig. 1(c): (i) a uniform configuration, where the DMI is equal across all layers, (ii) an enhanced DMI configuration, where the sign of the DMI aligns along the internal dipolar fields everywhere in the stack, and (iii) a reduced DMI configuration where the sign of the DMI is

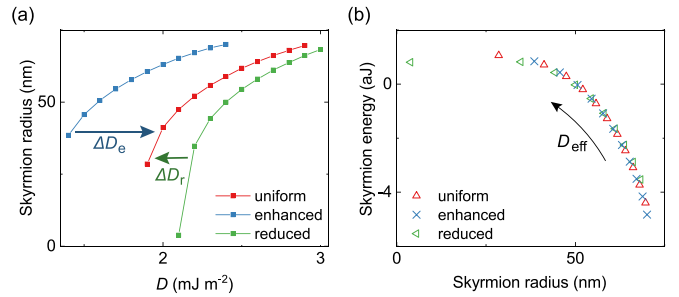


FIG. 2. (a) Skyrmion radii as function of D for three different DMI configurations with $N = 4$. The radius is determined from the position where the magnetization along the out-of-plane axis changes sign. (b) Skyrmion energy as a function of skyrmion radius for the three different DMI configurations with $N = 4$. The arrow indicates the direction of increasing D_{eff} .

always aligned antiparallel to the dipolar fields. The enhanced and reduced DMI configurations lead to the formation of a thickness-dependent chirality by the introduction of Néel caps. For all DMI configurations, the skyrmion energy decreases with increasing DMI as expected. In addition, the enhanced DMI configuration leads to a significantly reduced skyrmion energy, and the reduced configuration to an increase in the skyrmion energy. This is completely in line with the simple picture sketched in Fig. 1(a). Specifically, as indicated in Fig. 1(b) with the DMI gain ΔD_e , the D required to obtain a skyrmion whose energy is lower than the uniformly magnetized state decreases by 0.6 mJ m⁻² upon introducing the enhanced configuration. Similarly, for the reduced DMI configuration, this D increases by $\Delta D_r \approx 0.2$ mJ m⁻². The asymmetry between ΔD_e and ΔD_r is rather surprising in light of Fig. 1(a), but results from an additional contribution from the stray fields of the domain walls themselves that prefers to align the walls in the Néel cap configuration [30,31,40]. Nevertheless, the increase in the DMI for the enhanced configuration is large and comparable in magnitude to the gains obtained when utilizing an effect like additive DMI [13,18,41]. Moreover, as we are not bound to the small set of material systems with a large additive DMI, this should be more widely applicable. In Supplemental Material note II [34], we additionally show that while $\Delta D_{e,r}$ does vary with N , the presented behavior remains qualitatively identical.

Introducing these different DMI configurations also has a profound effect on the skyrmion radius, as shown in Fig. 2(a) [42]. In agreement with the results found in literature, an increase in D leads to an increase in the skyrmion radius [13,43]. We can understand this by thinking of a skyrmion as an out-of-plane magnetized core enclosed by a domain wall [43,44]. As D increases, the domain-wall energy decreases, resulting in a skyrmion that can expand to enhance the dipolar coupling of the core to the annulus. The same mechanism explains the behavior for the three different DMI configurations; the skyrmion becomes bigger (smaller) when introducing the enhanced (reduced) DMI configuration because the domain-wall energy decreases (increases). In Supplemental Material note IV [34], we further illustrate that the confinement effect of the simulated dot does not qualitatively affect the presented behavior.

We will now try to understand the effect of the different DMI configurations in a more general way. Combined, the behavior depicted in Figs. 1(b) and 2(a) suggests some form of universality. All the curves show qualitatively the same behavior as a function of D , apart from the shifted D values indicated by the arrows of DMI gain (ΔD_e) and loss (ΔD_r). This can be understood by considering the effect of the dipolar fields: as suggested by Lemesh *et al.*, [25] the dipolar fields can be included as an effective DMI because both components introduce an effective in-plane magnetic field in the domain wall. We can thus introduce an effective DMI $D_{\text{eff}} = D + \Delta D_{e,r}$ [see Fig. 1(b)] for the enhanced and reduced configurations. In this specific case, the enhanced configuration behaves as a system with an effective DMI D_{eff} , that is, $\Delta D_e \approx +0.6 \text{ mJ m}^{-2}$ larger than the DMI D because of the additive effects of the DMI and dipolar interactions. Conversely, the reduced configuration has a smaller effective DMI with $\Delta D_r \approx -0.2 \text{ mJ m}^{-2}$. A consequence of this universality is shown in Fig. 2(b), where the skyrmion energy is plotted as a function of skyrmion radius for the three different DMI configurations. The simulations for the different DMI configurations collapse on the same curve. Thus, although for each configuration the D needed to obtain a particular energy/radius is different, the relationship between the two remains unaffected and can be described by a D_{eff} that has a DMI-configuration dependent contribution. Lastly, in Supplemental Material note V [34], we demonstrate that the introduction of Néel caps can in some cases lead to noncircular skyrmions to accommodate both the DMI and dipolar interactions.

III. EXPERIMENTAL CONFIRMATION

In the previous section, we introduced the unique ability of a layer-dependent DMI configuration to enhance the stability of skyrmions. This section presents experimental evidence which shows that D_{eff} can be tailored by modifying the DMI on a layer-by-layer basis. To demonstrate this, instead of skyrmions we shift our attention to domain walls for their much easier experimental access, and their fully analogous underlying physics [24] (also see Supplemental Material note VI [34], where we simulate domain walls and demonstrate that they behave similar to skyrmions). They allow us to accurately quantify D_{eff} because the domain width d in magnetic multilayers is determined by the competition between the domain-wall energy and dipolar interactions between the domains [12–14,24,25,45–47]. Here, we use the accurate stripe domain model by Lemesh *et al.* [47] to determine D_{eff} in four different Ta(4)/Pt(2)/X/Ta(4) systems (thicknesses in parentheses in nanometers) to investigate the effect of the different DMI configurations. X for each stack is given by

$$\text{Uniform I : } \overbrace{[\text{Pt}(1)/\text{Co}(1)/\text{Ir}(1)]}^{+D} \times 4,$$

$$\text{Uniform II : } \overbrace{[\text{Ir}(1)/\text{Co}(1)/\text{Pt}(1)]}^{-D} \times 4,$$

$$\text{Enhanced : } \overbrace{[\text{Pt}(1)/\text{Co}(1)/\text{Ir}(1)]}^{+D} \times 2 \overbrace{[\text{Ir}(1)/\text{Co}(1)/\text{Pt}(1)]}^{-D} \times 2,$$

$$\text{Reduced : } \overbrace{[\text{Ir}(1)/\text{Co}(1)/\text{Pt}(1)]}^{-D} \times 2 \overbrace{[\text{Pt}(1)/\text{Co}(1)/\text{Ir}(1)]}^{+D} \times 2.$$

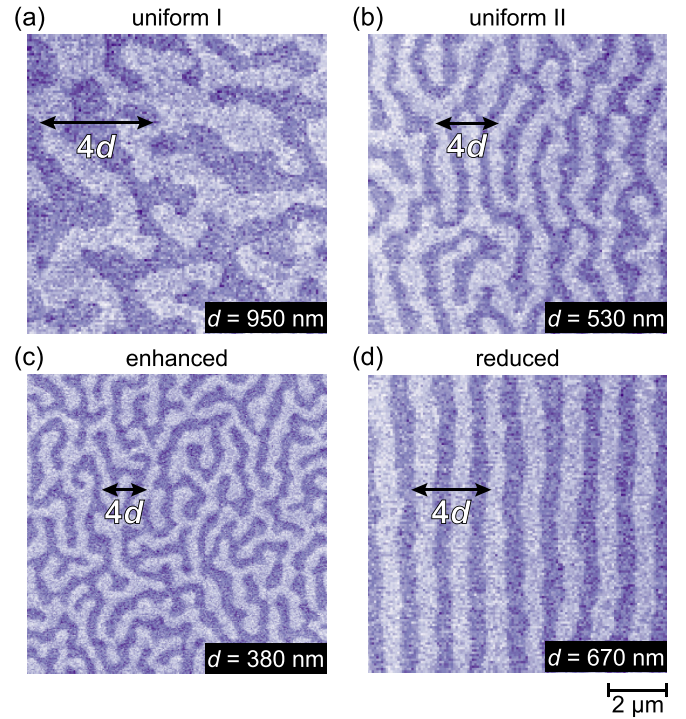


FIG. 3. MFM images of a demagnetized domain state for (a) the uniform I stack, (b) the uniform II stack, (c) the enhanced stack, and (d) the reduced stack. The scale bar at the bottom right holds for all figures. The arrows indicate the average domain width d , which we also show in the bottom right of each scan.

Pt and Ir were chosen because of their opposite interfacial DMI signs such that they favor CCW Néel walls for a Pt/Co/Ir stacking ($+D$) and CW Néel walls for an Ir/Co/Pt stacking ($-D$) [13,48–51]. The two different uniform stacks were fabricated to investigate the contributions of the stacking order. In Fig. 3, the resulting domain patterns after demagnetization are shown. These were recorded using magnetic force microscopy (MFM) measurements and the domain width d was extracted through a Fourier analysis. The experimental details can be found in Supplemental Material note I [34]

We start our discussion of the experimental results by looking at the enhanced and reduced configuration. For the enhanced configuration, we would expect a larger D_{eff} compared to reduced configuration because of the additive effect of the DMI and the dipolar interactions. From the measured domain widths d , we calculate D_{eff} and show this in Table I [47]. Indeed, D_{eff} is larger for the enhanced configuration (1.5 mJ m^{-2}) compared to the reduced configuration (0.9 mJ m^{-2}). As suggested earlier, this possibly results from the modified DMI ordering in combination with the dipolar interactions that lead to Néel caps.

There is another element that we have to account for in this analysis: the effect of the stacking order of the layers. For both uniform configurations, $|D_{\text{eff}}|$ should be equal as we have simply inverted the stacking order. However, as we calculate $|D_{\text{eff}}|$ from the measured d , we find that it varies by a factor of 2 for the uniform I and II configurations as shown in Table I. Moreover, there is also significant variation in the measured saturation magnetization M_s and anisotropy K for

TABLE I. Analysis of the domain widths d for the four different stacks extracted from Fig. 3. From these values, the effective DMI $|D_{\text{eff}}|$ was calculated using the accurate stripe domain model with $A = 10 \text{ pJ m}^{-1}$ [47]. The uniform averaged stack is a hypothetical stack with the average magnetic parameters of the uniform I and II stacks.

	d (nm)	M_s (MA m^{-1})	K (MJ m^{-3})	$ D_{\text{eff}} $ (mJ m^{-2})
Uniform I	$(9.5 \pm 0.4) \times 10^2$	0.93 ± 0.03	1.02 ± 0.04	1.3 ± 0.1
Uniform II	$(5.3 \pm 0.1) \times 10^2$	1.30 ± 0.05	1.60 ± 0.08	0.6 ± 0.2
Uniform averaged	–	1.12 ± 0.06	1.31 ± 0.09	1.0 ± 0.1
Enhanced	$(3.8 \pm 0.1) \times 10^2$	1.10 ± 0.04	1.31 ± 0.06	1.5 ± 0.1
Reduced	$(6.7 \pm 0.5) \times 10^2$	1.14 ± 0.04	1.31 ± 0.06	0.9 ± 0.2

these configurations. From this, we conclude that the magnetic parameters for [Pt/Co/Ir] and [Ir/Co/Pt] vary significantly because of growth-related effects stemming from the stacking order [52]. This seriously complicates the comparison between the different DMI configurations.

To still be able to compare the different DMI configurations, we need to extract the actual D values for the enhanced and reduced configurations to conclude if there is an increase in D_{eff} for these systems. For this, we account for the growth-induced variations quantitatively. We get a hint of how to do this by carefully looking at the data for M_s and K . The average M_s and K of both uniform stacks are $1.12 \pm 0.06 \text{ MA m}^{-1}$ and $1.31 \pm 0.09 \text{ MJ m}^{-3}$, respectively. This closely matches the experimental values for both the reduced and enhanced configurations. In other words, we can approximate these systems by looking at them as consisting of half a uniform I stack and half a uniform II stack. To calculate D for the enhanced and reduced configuration, we can therefore simply average the D_{eff} of both uniform configurations, which we have included in Table I.

We have carefully verified this approximation by performing micromagnetic simulations in Supplemental Material note VI [34]. In these simulations, we compare the domain-wall energies in the enhanced and reduced stack with layer-dependent magnetic parameters to a stack with the averaged parameters of both uniform stacks. From this, we conclude that a hypothetical stack with these averaged magnetic parameters is a good approximation of the experimental situation, leading to errors in $D_{\text{eff}} < 0.1 \text{ mJ m}^{-2}$.

We now compare D_{eff} of the averaged stack (1.0 pJ m^{-1}) to both the enhanced and reduced stack; we find that the absolute increase of the enhanced configuration ($+0.5 \text{ pJ m}^{-1}$) and decrease of the reduced configuration (-0.1 pJ m^{-1}) agree reasonably well with the values predicted in Fig. 1(b) of $\Delta D_e = +0.6 \text{ pJ m}^{-1}$ and $\Delta D_r = -0.2 \text{ pJ m}^{-1}$. Despite the growth-related complications when the building blocks of our stacks are reversed, we believe that our experimental results convincingly demonstrate that changing the sign of the DMI halfway through the stack leads to significant changes in D_{eff} . Finally, in Supplemental Material note VII [34], we present experimental results for an $N = 8$ system, with similar variations in D_{eff} as the $N = 4$ system proving the wide applicability of our approach.

Summarizing the experimental part, we found changing the sign of the DMI halfway through a multilayer system is a powerful method to increase the effective DMI. With the relatively modest increase in D_{eff} of the enhanced configuration

($1.5 \pm 0.1 \text{ mJ m}^{-2}$) compared to the uniform I configuration ($1.3 \pm 0.1 \text{ mJ m}^{-2}$), there is still room for improvement. The largest benefit of the enhanced DMI configuration will be found in a system with a large DMI where the growth-induced variations between the opposite stacking orders are small. As there are a host of different interface combinations with a large DMI, we expect there to be many material combinations that fit this pattern. Moreover, as we indicate in Supplemental Material note II [34], changing the amount of repeats can also lead to larger increases in the effective DMI. Lastly, we also expect that varying the thickness of the nonmagnetic layer could be used to further optimize the effective DMI.

IV. DISCUSSION AND CONCLUSION

We would now like to comment on two aspects of exploiting the Néel caps to stabilize chiral spin structures. First, the introduction of an enhanced DMI configuration does not affect the skyrmion dynamics. Although the resulting vanishing total interfacial chirality suggests that spin-orbit torques can no longer be used to drive skyrmion dynamics, this is not true for the proposed experimental stacks of [Pt/Co/Ir] and [Ir/Co/Pt] [24–26,53]. When changing the stacking order halfway through the stack, it is not only the interfacial chirality but also the local spin-orbit torques from the individual Pt and Ir layers that are reversed [54]. In this case, the spin-orbit torques acting on the skyrmion are the same for both halves of the stacks, ensuring skyrmions can still be driven efficiently using an electrical current. As there are also indications that an enhanced DMI configuration can postpone the Walker-breakdown-like behavior for both domain walls and skyrmions to much higher current densities [55], it is therefore interesting to explore their dynamics in the case of an enhanced DMI configuration in more detail.

Second, more ideas exist that make use of dipolar interactions and magnetic parameters that vary on a layer-by-layer basis. For example, by modifying the anisotropy, one might be able to increase the domain-wall width at the top and bottom of the film to enhance the coupling with the dipolar fields and increase the skyrmion stability even further. Or one could imagine changing the position within the stack where the DMI reverses, and thus the point at which the chirality reverses, to, for example, reduce the skyrmion Hall angle [26]. Perhaps it is even possible to stabilize more complex three-dimensional spin structures such as the magnetic hopfion or skyrmion bobber by modifying individual magnetic parameters on a layer-by-layer basis [56–58].

In conclusion, using micromagnetic simulations we have shown that the stability of chiral spin structures in multilayer systems can be significantly enhanced by exploiting the presence of Néel caps. This can be done by introducing an alternating DMI in a multilayer system, leading to increases in the effective DMI of at least 0.6 mJ m^{-2} . We have also shown experimental results in this direction, where we find variations in the effective DMI that agree with our predictions. These results open the way to alternative methods for the

stabilization of chiral spin structures by tailoring the magnetic interactions on a layer-by-layer basis.

ACKNOWLEDGMENTS

This work is part of the research program of the Foundation for Fundamental Research on Matter (FOM), which is part of the Netherlands Organisation for Scientific Research (NWO).

-
- [1] N. Nagaosa and Y. Tokura, *Nat. Nanotechnol.* **8**, 899 (2013).
- [2] R. Wiesendanger, *Nat. Rev. Mater.* **1**, 16044 (2016).
- [3] A. Fert, N. Reyren, and V. Cros, *Nat. Rev. Mater.* **2**, 17031 (2017).
- [4] K. Everschor-Sitte, J. Masell, R. M. Reeve, and M. Kläui, *J. Appl. Phys.* **124**, 240901 (2018).
- [5] S. Rohart, J. Miltat, and A. Thiaville, *Phys. Rev. B* **93**, 214412 (2016).
- [6] A. Fert, V. Cros, and J. Sampaio, *Nat. Nanotechnol.* **8**, 152 (2013).
- [7] T. Moriya, *Phys. Rev.* **120**, 91 (1960).
- [8] I. Dzyaloshinsky, *J. Phys. Chem. Solids* **4**, 241 (1958).
- [9] S. Mühlbauer, B. Binz, F. Jonietz, C. Pfleiderer, A. Rosch, A. Neubauer, R. Georgii, and P. Böni, *Science* **323**, 915 (2009).
- [10] X. Z. Yu, Y. Onose, N. Kanazawa, J. H. Park, J. H. Han, Y. Matsui, N. Nagaosa, and Y. Tokura, *Nature* **465**, 901 (2010).
- [11] S. Heinze, K. von Bergmann, M. Menzel, J. Brede, A. Kubetzka, R. Wiesendanger, G. Bihlmayer, and S. Blügel, *Nat. Phys.* **7**, 713 (2011).
- [12] S. Woo, K. Litzius, B. Krüger, M.-Y. Im, L. Caretta, K. Richter, M. Mann, A. Krone, R. M. Reeve, M. Weigand, P. Agrawal, I. Lemesh, M.-A. Mawass, P. Fischer, M. Kläui, and G. S. D. Beach, *Nat. Mater.* **15**, 501 (2016).
- [13] C. Moreau-Luchaire, C. Moutafis, N. Reyren, J. Sampaio, C. A. F. Vaz, N. Van Horne, K. Bouzehouane, K. Garcia, C. Deranlot, P. Warnicke, P. Wohlhüter, J.-M. George, M. Weigand, J. Raabe, V. Cros, and A. Fert, *Nat. Nanotechnol.* **11**, 444 (2016).
- [14] O. Boulle, J. Vogel, H. Yang, S. Pizzini, D. d. S. Chaves, A. Locatelli, T. O. M. A. Sala, L. D. Buda-Prejbeanu, O. Klein, M. Belmeguenai, Y. Roussigné, A. Stashkevich, S. M. Chérif, L. Aballe, M. Foerster, M. Chshiev, S. Auffret, I. M. Miron, and G. Gaudin, *Nat. Nanotechnol.* **11**, 449 (2016).
- [15] A. N. Bogdanov and U. K. Röbber, *Phys. Rev. Lett.* **87**, 037203 (2001).
- [16] A. Fert, *Metallic Multilayers*, Materials Science Forum, Vol. 59 (Trans Tech Publications Ltd., 1991), pp. 439–480.
- [17] A. Crépieux and C. Lacroix, *J. Magn. Magn. Mater.* **182**, 341 (1998).
- [18] A. Soumyanarayanan, M. Raju, A. L. Gonzalez Oyarce, A. K. C. Tan, M.-Y. Im, A. P. Petrovic, P. Ho, K. H. Khoo, M. Tran, C. K. Gan, F. Ernult, and C. Panagopoulos, *Nat. Mater.* **16**, 898 (2017).
- [19] A. Hubert and R. Schäfer, *Magnetic Domains: the Analysis of Magnetic Microstructures*, 1st ed. (Springer-Verlag, Berlin, 1998), pp. 240–241.
- [20] J. Lucassen, M. J. Meijer, O. Kurnosikov, H. J. M. Swagten, B. Koopmans, R. Lavrijsen, F. Kloodt-Twesten, R. Frömter, and R. A. Duine, *Phys. Rev. Lett.* **123**, 157201 (2019).
- [21] W. Li, I. Bykova, S. Zhang, G. Yu, R. Tomasello, M. Carpentieri, Y. Liu, Y. Guang, J. Gräfe, M. Weigand, D. M. Burn, G. van der Laan, T. Hesjedal, Z. Yan, J. Feng, C. Wan, J. Wei, X. Wang, X. Zhang, H. Xu, C. Guo, H. Wei, G. Finocchio, X. Han, and G. Schütz, *Adv. Mater.* **31**, 1807683 (2019).
- [22] J. A. Garlow, S. D. Pollard, M. Beleggia, T. Dutta, H. Yang, and Y. Zhu, *Phys. Rev. Lett.* **122**, 237201 (2019).
- [23] S. A. Montoya, S. Couture, J. J. Chess, J. C. T. Lee, N. Kent, D. Henze, S. K. Sinha, M.-Y. Im, S. D. Kevan, P. Fischer, B. J. McMorran, V. Lomakin, S. Roy, and E. E. Fullerton, *Phys. Rev. B* **95**, 024415 (2017).
- [24] W. Legrand, J.-Y. Chauleau, D. Maccariello, N. Reyren, S. Collin, K. Bouzehouane, N. Jaouen, V. Cros, and A. Fert, *Sci. Adv.* **4**, eaat0415 (2018).
- [25] I. Lemesh and G. S. D. Beach, *Phys. Rev. B* **98**, 104402 (2018).
- [26] W. Legrand, N. Ronceray, N. Reyren, D. Maccariello, V. Cros, and A. Fert, *Phys. Rev. Appl.* **10**, 064042 (2018).
- [27] Y. Dovzhenko, F. Casola, S. Schlotter, T. X. Zhou, F. Büttner, R. L. Walsworth, G. S. D. Beach, and A. Yacoby, *Nat. Commun.* **9**, 2712 (2018).
- [28] K. Fallon, S. McVitie, W. Legrand, F. Ajejas, D. Maccariello, S. Collin, V. Cros, and N. Reyren, *Phys. Rev. B* **100**, 214431 (2019).
- [29] As the chirality of the skyrmions varies between individual repeats of the multilayer system, these are not skyrmions in the strictest sense [1–4].
- [30] A. Hrabec, J. Sampaio, M. Belmeguenai, I. Gross, R. Weil, S. M. Chérif, A. Stashkevich, V. Jacques, A. Thiaville, and S. Rohart, *Nat. Commun.* **8**, 15765 (2017).
- [31] A. Bellec, S. Rohart, M. Labrune, J. Miltat, and A. Thiaville, *EPL* **91**, 17009 (2010).
- [32] M. J. Meijer, J. Lucassen, O. Kurnosikov, H. J. M. Swagten, B. Koopmans, R. Lavrijsen, F. Kloodt-Twesten, R. Frömter, and R. A. Duine, *Phys. Rev. Lett.* **124**, 207203 (2020).
- [33] A. Vansteenkiste, J. Leliaert, M. Dvornik, M. Helsen, F. Garcia-Sanchez, and B. Van Waeyenberge, *AIP Adv.* **4**, 107133 (2014).
- [34] See Supplemental Material at <http://link.aps.org/supplemental/10.1103/PhysRevB.102.014451> for I. Methods, II. Simulations for different repeats, III. Information on magnetic field dependence, IV. Simulations for a smaller dot, V. Non-circular skyrmions, VI. Validation of the averaging approach,

- and VII. experimental results for an 8-repeat stack. It additionally includes Refs. [35–39].
- [35] S. Hosaka, A. Kikukawa, Y. Honda, H. Koyanagi, and S. Tanaka, *Jpn. J. Appl. Phys.* **31**, L904 (1992).
- [36] J. Lucassen, F. Kloedt-Twesten, R. Frömter, H. P. Oepen, R. A. Duine, H. J. M. Swagten, B. Koopmans, and R. Lavrijsen, *Appl. Phys. Lett.* **111**, 132403 (2017).
- [37] M. T. Johnson, P. J. H. Bloemen, F. J. A. den Broeder, and J. J. de Vries, *Rep. Prog. Phys.* **59**, 1409 (1996).
- [38] R. F. L. Evans, W. J. Fan, P. Chureemart, T. A. Ostler, M. O. A. Ellis, and R. W. Chantrell, *J. Phys.: Condens. Matter* **26**, 103202 (2014).
- [39] A. De Lucia, K. Litzius, B. Krüger, O. A. Tretiakov, and M. Kläui, *Phys. Rev. B* **96**, 020405 (2017).
- [40] J.-P. Tetienne, T. Hingant, L. J. Martínez, S. Rohart, A. Thiaville, L. H. Diez, K. Garcia, J.-P. Adam, J.-V. Kim, J.-F. Roch, I. M. Miron, G. Gaudin, L. Vila, B. Ocker, D. Ravelosona, and V. Jacques, *Nat. Commun.* **6**, 6733 (2015).
- [41] H. Yang, O. Boule, V. Cros, A. Fert, and M. Chshiev, *Sci. Rep.* **8**, 12356 (2018).
- [42] In Supplemental Material at <http://link.aps.org/supplemental/10.1103/PhysRevB.102.014451> note III [34], we also show the results for the simulations under an applied magnetic field, where the enhanced DMI configuration leads to a larger field stability.
- [43] S. Rohart and A. Thiaville, *Phys. Rev. B* **88**, 184422 (2013).
- [44] N. Romming, A. Kubetzka, C. Hanneken, K. von Bergmann, and R. Wiesendanger, *Phys. Rev. Lett.* **114**, 177203 (2015).
- [45] H. J. G. Draaisma and W. J. M. De Jonge, *J. Appl. Phys.* **62**, 3318 (1987).
- [46] A. Suna, *J. Appl. Phys.* **59**, 313 (1986).
- [47] I. Limesh, F. Büttner, and G. S. D. Beach, *Phys. Rev. B* **95**, 174423 (2017).
- [48] X. Ma, G. Yu, C. Tang, X. Li, C. He, J. Shi, K. L. Wang, and X. Li, *Phys. Rev. Lett.* **120**, 157204 (2018).
- [49] S. Tacchi, R. E. Troncoso, M. Ahlberg, G. S. D. Gubbiotti, M. Madami, J. Åkerman, and P. Landeros, *Phys. Rev. Lett.* **118**, 147201 (2017).
- [50] D.-S. Han, N.-H. Kim, J.-S. Kim, Y. Yin, J.-W. Koo, J. Cho, S. Lee, M. Kläui, H. J. M. Swagten, B. Koopmans, and C.-Y. You, *Nano Lett.* **16**, 4438 (2016).
- [51] S. Finizio, S. Wintz, K. Zeissler, A. V. Sadovnikov, S. Mayr, S. A. Nikitov, C. H. Marrows, and J. Raabe, *Nano Lett.* **19**, 375 (2019).
- [52] S. Bandiera, R. C. Sousa, B. Rodmacq, and B. Dieny, *IEEE Magn. Lett.* **2**, 3000504 (2011).
- [53] S. A. Montoya, R. Tolley, I. Gilbert, S.-G. Je, M.-Y. Im, and E. E. Fullerton, *Phys. Rev. B* **98**, 104432 (2018).
- [54] A. Manchon, J. Železný, I. M. Miron, T. Jungwirth, J. Sinova, A. Thiaville, K. Garello, and P. Gambardella, *Rev. Mod. Phys.* **91**, 035004 (2019).
- [55] I. Limesh and G. S. Beach, *Phys. Rev. Applied* **12**, 044031 (2019).
- [56] X. S. Wang, A. Qaiumzadeh, and A. Brataas, *Phys. Rev. Lett.* **123**, 147203 (2019).
- [57] Jung-Shen B. Tai and I. I. Smalyukh, *Phys. Rev. Lett.* **121**, 187201 (2018).
- [58] P. Sutcliffe, *J. Phys. A* **51**, 375401 (2018).